Cyclic deformation mechanisms and microcracks behavior in high-strength bainitic steel

M.C. Marinelli, I. Alvarez-Armas, U. Krupp

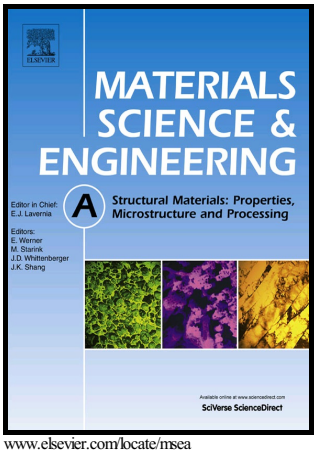

www.elsevier.com/locate/msea

PII: S0921-5093(16)31498-8
DOI: http://dx.doi.org/10.1016/j.msea.2016.12.018
Reference: MSA34449

To appear in: *Materials Science & Engineering A*

Received date: 22 August 2016
Revised date: 2 December 2016
Accepted date: 3 December 2016

Cite this article as: M.C. Marinelli, I. Alvarez-Armas and U. Krupp, Cyclic deformation mechanisms and microcracks behavior in high-strength bainitic steel *Materials Science & Engineering A* http://dx.doi.org/10.1016/j.msea.2016.12.018

Cyclic deformation mechanisms and microcracks behavior in high-strength bainitic steel

M.C. Marinelli[a]*, I. Alvarez-Armas[a], U. Krupp[b]

[a]Instituto de Física Rosario – Consejo Nacional de Investigaciones Científicas y Técnicas (CONICET), Universidad Nacional de Rosario, Argentina

[b]Faculty of Engineering and Computer Science, University of Applied Sciences Osnabrück, Germany

*Corresponding author. Tel.: +54-341 485 3200. E-mail: marinelli@ifir-conicet.gov.ar

Abstract

The purpose of this investigation is to analyze the mechanisms of cyclic deformation and the initiation and propagation of microcracks during low cycle fatigue in the bainitic steel 16CrMnV7-7. The slip systems and their associated Schmid Factor are analyzed in the bainitic ferrite laths and correlated with the short crack path using scanning electron microscopy observations (SEM) in combination with electron backscattered diffraction (EBSD) measurements. Moreover, the developed dislocation structure was analyzed and correlated with the formation and propagation of microcracks. The principal results show that microcracks initiate in lath boundaries and along slip systems with the highest Schmid Factor and low Taylor Factor. Besides, it was observed after experimental evidence that the parameters controlling crack propagation are associated with the crystallographic misorientation between bainite blocks and with the tilt/twist misorientation angle between slip planes of adjacent bainitic ferrite laths.

Keywords: Low cycle fatigue, high strength bainitic steel, microstructure, initiation and propagation crack

1. Introduction

The high strength bainitic steels are important in many applications in the automobile industry as crash reinforcement bars to protect against sidewise impact and for injection lines (under pulsating loads) in common rail diesel engines [1]. The microstructure of these steels consists of blocks or sheaves which are divided into sub-micrometer laths of bainitic ferrite with similar crystallographic orientation and with high density of dislocation separated by carbon-enriched regions of austenite with or without martensite [2-5]. The cementite particles are responsible for the limited application of conventional bainitic steels, however, it has been verified that the cementite precipitation during bainitic transformation can be suppressed by alloying the steel with silicon, which has very low solubility in cementite and greatly retards growth of cementite from austenite. New research [3-7] showed that the high strength of bainitic steels is achieved reducing the thickness of the bainitic ferrite laths. Nowadays, the research is focused on reaching bainitic ferrite laths increasingly thin to obtain better mechanical properties [8 -12]. In order to fully exploit the potential of bainitic steels in industrial applications, a better understanding must be achieved on the fatigue behaviour and failure. Although most applications of structural materials involve cyclic loading, only limited amount of research concerning low cycle fatigue behavior and fatigue cracks in these types of steels have been reported.

Bhambri et al. [13] reported that Cr-Mo-0.25V turbine rotor steel with bainite and ferrite microstructure softens continuously. Sankaran et al. and Padmanabhan and Sankaram [14, 15] in a high strength ferritic/bainitic/martensitic steel found that the retained austenite films between the bainitic ferrite laths prevent the cyclic softening.

Recently, Zhang et al. and Zhou et al. [9, 16] analyzed the cyclic behavior of low-carbon carbide-free bainitic steel in a range of strain amplitudes. They observed an initial cyclic hardening followed by saturation at lower strain amplitudes ($\Delta\varepsilon_t < 0.8\%$) or followed by cyclic softening at higher strain amplitudes ($\Delta\varepsilon_t > 0.8\%$). Although the authors proposed a decrease of the mobile dislocation density to explain the initial cyclic hardening, the cyclic mechanisms involved in the fatigue process are not completely clear yet.

On the other hand, concerning to crack initiation and eventually the mode of propagation in high strength bainitic steels, some authors [14-18] have studied the fracture surface reporting that the microcracks initiate along slip bands and show transgranular propagation.

As far as we know, no experimental microcrack characterization in the nucleation and propagation stage has been found in the literature in high strength bainitic steels. Therefore, the purpose of the present work is twofold: first to correlate the cyclic behavior and the developed microstructure in order to propose the deformation mechanism at intermediate and high plastic strain range. Secondly, we will focus our attention on the microstructural characterization of microcrack initiation and propagation in the intermediate strain range.

2. Material and experimental procedure

2.1. *Material*

The material considered in this work is the bainitic steel 16CrMnV7-7 with a nominal chemical composition as given in Table 1. The material was supplied by Georgsmarienhütte Steel (Germany) in the form of hot-rolled cylindrical bars of 30 mm in diameter. The martensite start temperature (Ms) is 420ºC and the bainite start

temperature is 500ºC. Optimal material properties are achieved by a tempered in a molten salt at a temperature of 350 ºC for 120 second obtaining lower bainite.

Table 1: Nominal chemical composition of the 16CrMnV7-7 (in wt. %). M_s= 420ºC

C	Si	Mn	P	S	Al	Sn
0.15-0.20	0.20-0.30	1.68-1.80	< 0.015	0.010-0.020	0.018-0.028	< 0.020
Cr	**Mo**	**Ni**	**V**	**Nb**	**N**	**Cu**
0.70-1.80	0.03-0.06	0.12-0.25	0.05-0.15	0.020-0.040	0.018-0.025	< 0.20

2.2. *Test specimen preparation*

The tests were carried out on cylindrical specimens and shallow notched cylindrical specimens (Fig. 1). Cylindrical specimens for fatigue life test were manufactured and polished in the test section with sequentially finer grits down to 1μm diamond paste to achieve a smooth surface. On the other hand, in the shallow notched cylindrical specimens, the surface of the shallow notch was mechanically and electrolytically polished using a solution 10% perchloric in ethanol to improve the observation of microcrack nucleation and growth. The central part of the notch was monitored during the test using an in situ optical system consisting of a CCD camera, JAI model CM-140MCL with a 50X objective, ± 1μm FD and 13mm WD and a 12X ultra zoom.

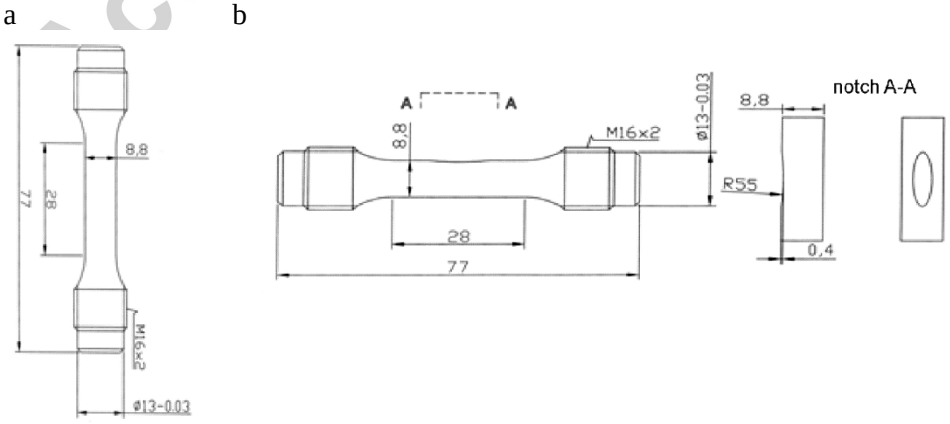

Figure 1: a) Cylindrical specimen, b) shallow notched specimen.

2.3. *Low cycle fatigue test conditions*

Push-pull fatigue tests were performed at room temperature on a testing machine INSTRON 1362. The fatigue tests were carried out under constant plastic strain amplitude of $\Delta\varepsilon_p = 0.2\%$ and $\Delta\varepsilon_p = 0.3\%$ with a fully reversed triangular wave and total strain rate of $2x10^{-3}s^{-1}$.

2.4. *Specimen preparation for microstructure analysis*

X-ray diffraction (XRD) analysis was employed for the detection of retained austenite in the as-received steel. XRD tests were performed using a Philips X'Pert Pro MPD diffractometer, equipped with a Cu Kα tube. Automated electron back scatter diffraction (EBSD) was used to determine the distribution of the phases and the crystallographic orientation as well as the size of bainitic ferrite blocks. The samples for XRD and EBSD analysis were ground to 2000 grit paper, followed by electro polishing with a solution of 10% perchloric acid and 90% ethanol at T = -15 °C , V=10V , I =1A and t = 4 min.

Internal dislocation structures were studied by transmission electron microscopy (TEM) in a Philips CM 200 transmission electron microscope operated at 160 kV. Thin foils were prepared from slices taken perpendicular to the stress axis of the fatigued cylindrical specimens. The discs of 3mm in diameter were subsequently thinned and electro polished in a twin-jet polishing unit using a 10% perchloric acid and 90% ethanol mixture at -17 °C and 20 V.

3. Results

3.1. *Characterization of the as-received microstructure*

The constituent phases of the as-received material were analyzed by XRD using Rietveld analysis by Powder cell 2.4. Fig. 2 shows the X-ray patterns indicating a 95 Vol.% of bainitic ferrite and 5 Vol.% of retained austenite. The retained austenite was

found between blocks and laths of bainitic ferrite as shows the phase map obtained by EBSD in Fig. 3.

A more detailed study made by TEM has revealed a fine dispersion of cementite precipitates in the matrix of the bainitic ferrite laths. This density of precipitates is relatively low and thus difficult to be detected by XRD. Fig. 4 shows a bright field and dark field image with the corresponding selected area electron diffraction patterns. The double points in the electron diffraction patterns corresponding to $\{111\}_\gamma$ and $\{110\}_\alpha$ planes indicate the coexistence of both austenite and ferrite phases. Moreover, in this dark field image the retained austenite and the cementite precipitation can be clearly observed. Additionally, the bright field image shows a homogeneous distribution of dislocations in the bainitic ferrite as is observed in Fig. 4a.

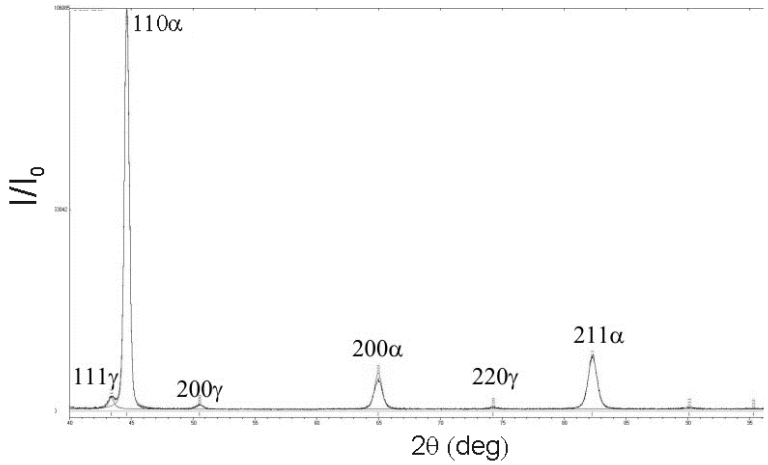

Figure 2: X-ray patterns indicating a 95 Vol.% of bainitic ferrite and 5 Vol.% of retained austenite.

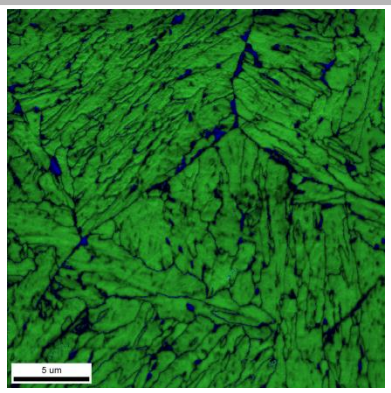

Figure 3: EBSD map indicating the bainitic steel phases: green for bainitic ferrite and blue for retained austenite.

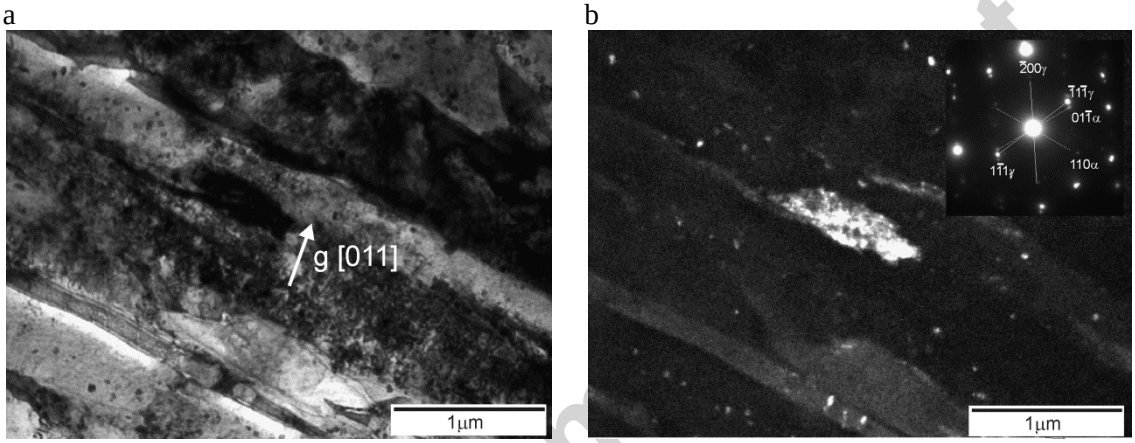

Figure 4: TEM microstructure of bainitic steel 16CrMnV7-7 a) bright field image showing lath of bainitic ferrite with a high density of dislocations. b) Corresponding dark field image (obtained with the double diffraction point:$(\bar{1}1\bar{1})_\gamma$ and $(01\bar{1})_\alpha$) with electron diffraction patterns showing retained austenite and cementite precipitates.

3.2. *Mechanical behavior*

The cyclic behavior of the bainitic steel 16CrMnV7-7 at room temperature under plastic-strain control for $\Delta\varepsilon_p$= 0.2% and $\Delta\varepsilon_p$ = 0.3% is shown in Fig. 5. Regardless of the imposed strain range, both curves show a short initial cyclic hardening stage, followed by a continuous cyclic softening that ends in a state of quasi-saturation.

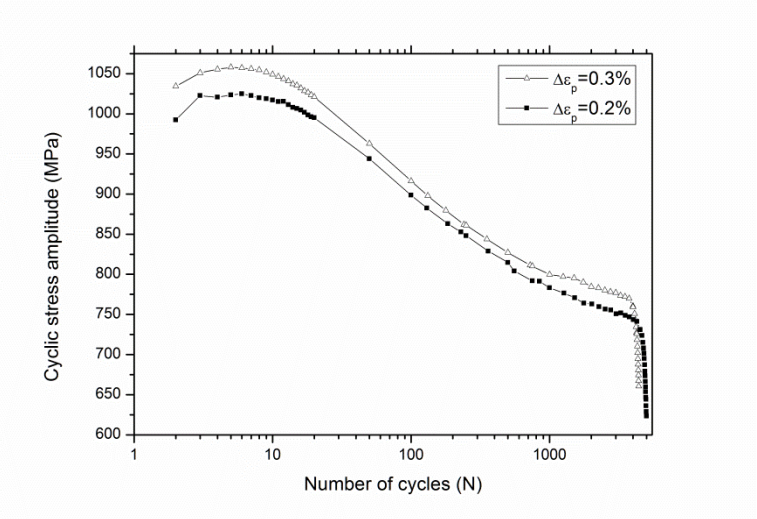

Figure 5: Cyclic stress amplitude vs number of cycles curve of fatigue sample at $\Delta\varepsilon_p$= 0.2% and $\Delta\varepsilon_p$= 0.3%.

3.3. *Microstructural evolution*

At intermediate plastic strain range, $\Delta\varepsilon_p$= 0.2%, the characteristic dislocation arrangement corresponds to heterogeneous distribution of loop patches of dislocations within the bainitic ferrite laths (Fig. 6a) at the end of the fatigue life. However, in some laths a dislocation arrangement in the form of ill-formed cell structure is observed (Fig. 6b). Furthermore, it is interesting to note that the lath boundaries and the cementite particles act as barriers against slip transmission into adjacent lath (Fig. 6a).

a

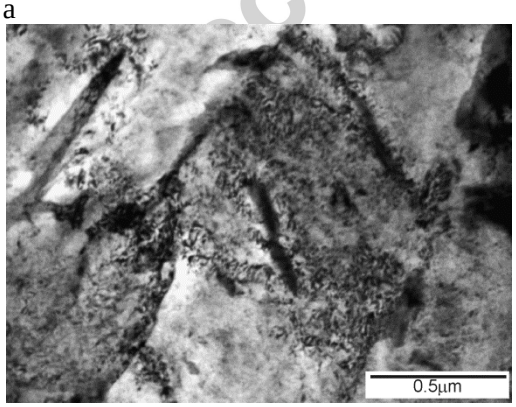

b

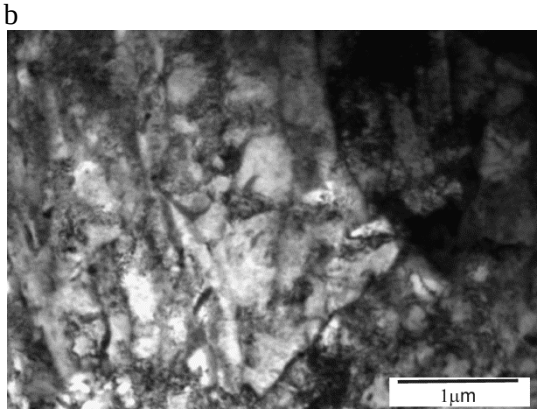

Figure 6: TEM micrograph of bainitic steel 16CrMnV7-7 fatigued at $\Delta\varepsilon_p$= 0.2%, N=5500cycles. a) Heterogeneous distribution of loop patches of dislocations into the bainitic ferrite lath, b) ill-formed cell structure.

At high plastic strain range, $\Delta\varepsilon_p$= 0.3%, the characteristic dislocation structure developed within the bainitic ferrite laths corresponds to well-formed cell with a mean diameter of 0.4μm (Fig. 7a) as well as wall dislocation structures (Fig. 7b) at the end of the fatigue life.

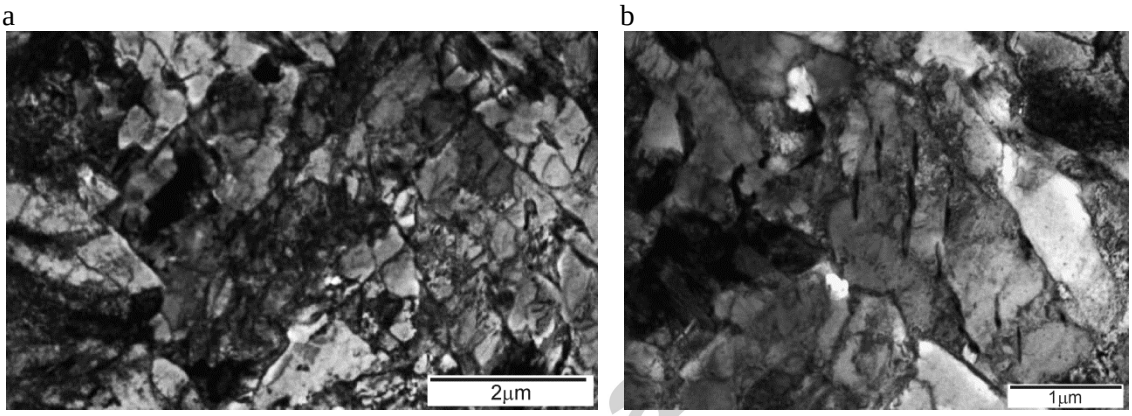

Figure 7: a) Well-formed cell and b) wall dislocation structure at $\Delta\varepsilon_p$= 0.3%, N=4400 cycles.

3.4. *Surface damage evolution*

In order to analyze the initiation and propagation of microcracks at $\Delta\varepsilon_p$= 0.2%, the central part of the notch was monitored and digitally recorded during the fatigue test. The slip systems were analyzed using a method quoted in [19].

The Fig 8 shows the evolution of surface damage where the first slip lines start after 20 cycles (indicated by arrows in Fig. 8b) and as cycling proceeds, these lines intensify leading to the microcracks initiation after 100 cycles (Fig. 8c). Fig 8d shows an important number of microcracks that remain arrested during cycling (which are

indicated by circles) and other microcracks identified as f_1, f_2 y f_3 which finally coalesce into the long crack.

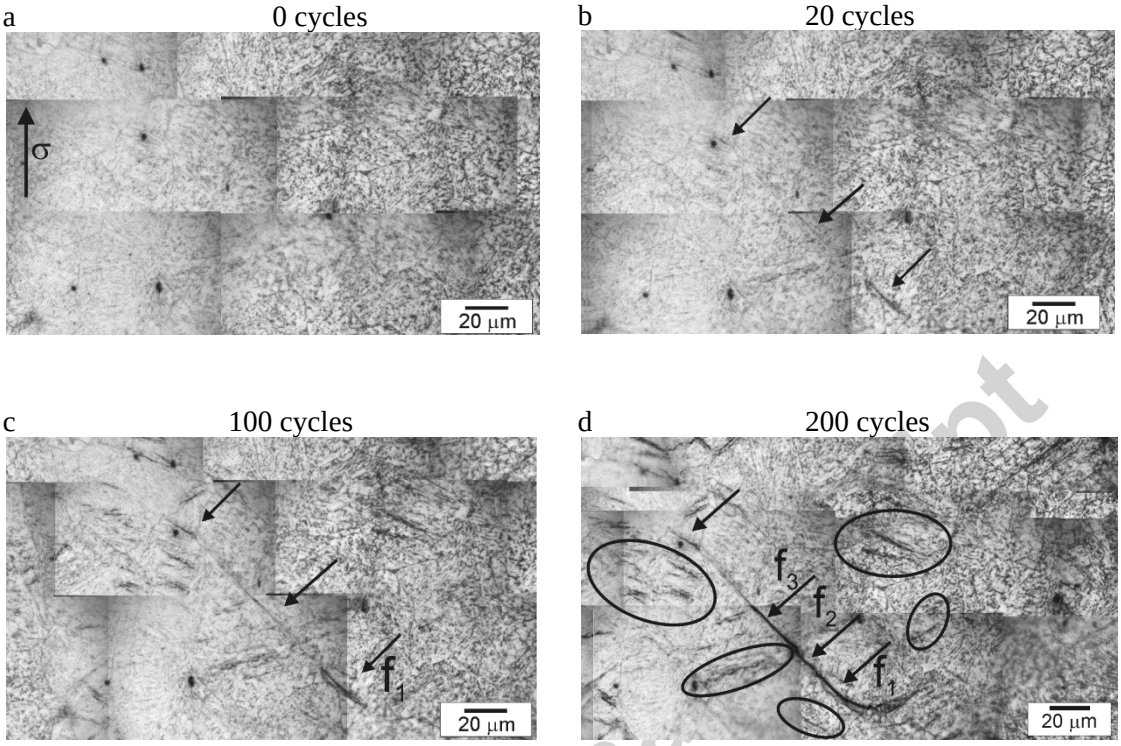

Figure 8: Evolution of short crack propagation at $\Delta\varepsilon_p$=0.2%.

According to Marinelli et al. [20] microcracks initiate in bainitic ferrite laths on the primary slip system {110}[111] favorable oriented with the highest Schmid Factor (SF). However, observing Fig. 9a, not all bainitic ferrite laths having high Smith Factor present microcracks. In order to elucidate this point, the Taylor Factor (TF) map was used in this analysis. As it is well-known, the Taylor Factor is a geometric factor which describes the ability of a crystal to slip (or not slip) based on the orientation of the crystal relative to the sample reference frame. Grains with low TF value are associated with low yield strength and can be deformed at lower stresses. In Fig. 9b, the laths in blue are oriented for relatively easy slip, while those in red tend to resist yielding process.

a b

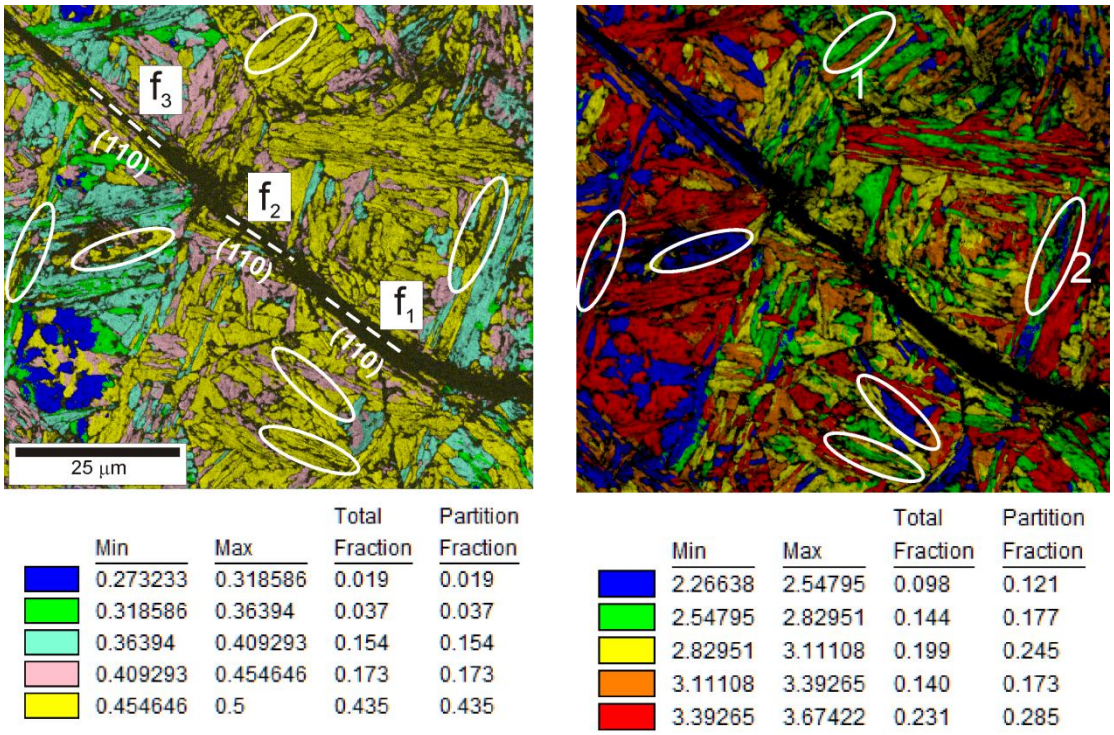

	Min	Max	Total Fraction	Partition Fraction
	0.273233	0.318586	0.019	0.019
	0.318586	0.36394	0.037	0.037
	0.36394	0.409293	0.154	0.154
	0.409293	0.454646	0.173	0.173
	0.454646	0.5	0.435	0.435

	Min	Max	Total Fraction	Partition Fraction
	2.26638	2.54795	0.098	0.121
	2.54795	2.82951	0.144	0.177
	2.82951	3.11108	0.199	0.245
	3.11108	3.39265	0.140	0.173
	3.39265	3.67422	0.231	0.285

Figure 9: a) Schmid Factor map and b) Taylor Factor map obtained by TSL OIM analysis after 900 cycles at $\Delta\varepsilon_p = 0.2\%$.

Concerning to microcrack nucleation, two sites of crack initiation can be identified: a) along the boundary between blocks or laths and b) into the bainitic ferrite lath on the trace of slip system with the highest SF and low TF. Fig. 10 shows an enlarged area of Fig. 9b showing the misorientation profile of microcrack 1 and 2 along a line crossing perpendicularly adjacent laths. The red and blue lines indicate the point-to-point as well as the point-to-origin misorientation measurements on this line.

From the point-to-origin profile in microcrack 1(Fig.10a), it can be seen that the lath with high TF is highly misorientated with respect to the two adjacent laths with lower TF; in this case the microcrack nucleates on one of the lath boundary. On the other hand, the point-to-origin profile in microcrack 2 (Fig. 10b) exhibits a peak associated with the existence of a microcrack. In this case, the microcrack 2 nucleates within the bainitic lath with low TF and favorable SF for the activation of the primary slip system.

In order to analyze the microcrack propagation a detailed monitoring on the notched area of the specimen was performed in situ during the fatigue test. The results show that some of the primary microcracks nucleate individually in slip planes/bands in the laths and the process of crack propagation occurs by coalescence of these mechanically nucleated microcracks at the surface. This process is exhibited in Fig 8d and Fig 9a in which three microcracks identified as f_1, f_2 y f_3 form in the early stage of the fatigue life. More precisely, they nucleated after 100 cycles on the slip system $(110) < \bar{1}11 >$ with SF= 0.48 and SF= 0.45 for f_1 and f_3 respectively, and $(110) < 1\bar{1}1 >$ with SF= 0.46 for f_2 and coalesced into the long crack after 200 cycles (Fig 8d).

a

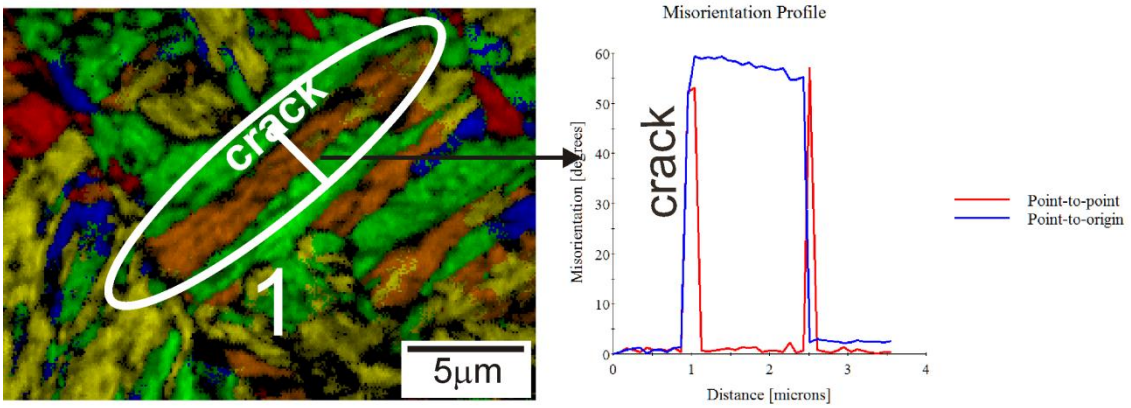

b

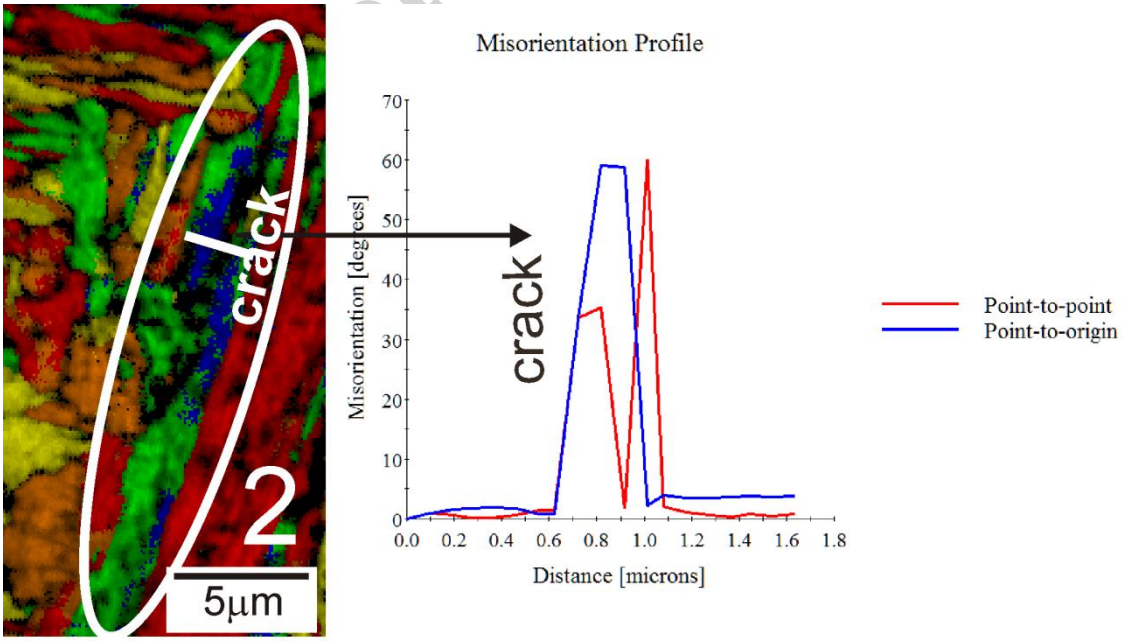

Figure 10: TF map and misorientation profile. a) Crack initiation between lath boundaries with low (green) and high (orange) TF. b) Crack initiation in bainitic ferrite lath orientated on the slip system $(0\bar{1}1)$ <111> with the highest SF and low TF.

4. Discussion

In the present paper the cyclic behavior of bainitic steel 16CrMnV7-7 at plastic strain amplitudes of $\Delta\varepsilon_p$= 0.2% and $\Delta\varepsilon_p$ = 0.3% was studied and correlated with the microstructure and this result was additionally used to analyze the initiation and propagation out of the crack.

The initial cyclic hardening observed in Fig. 5 can be attributed to interaction of preexisting dislocations with cementite particles producing different pinning mechanism. On the other hand, the cyclic softening is associated with the annihilation and rearrangement of the dislocations as it happens in other steels with high initial dislocation density such as tempering martensitic steels [21].

In the present steel, the characteristic dislocations structure developed at $\Delta\varepsilon_p$ = 0.3% correspond to well-formed cell structure (Fig. 7a) while at $\Delta\varepsilon_p$ = 0.2% the dislocations arrange in the form of loop patches and ill-formed cell structures (Fig 6). As a matter of fact, the formation of this incipient (ill-formed cells) dislocation structure as well as the final one (well-formed cells) indicate that a process of rearrangement of dislocation exists and can be considered as the origin of the cyclic softening.

With respect to the fatigue crack, the slip systems, Schmid Factor and Taylor Factor were analyzed using EBSD. According to this study, the microcracks can nucleate within bainitic ferrite laths on primary the slip system {110}[111] favorable to slip with the highest SF and low TF (Fig 10b). Alternatively, microcracks can also nucleate between bainitic ferrite laths or blocks highly misorientated (Fig 10a). In the first case, a

lath with low TF and high SF shows easy slip for dislocations which favorable contributes to the formation of extrusion/intrusion in the near-surface laths. Conversely, with respect to crack initiation in the lath boundary, Fig 10a shows this situation in which the laths have low and high TF, respectively. As a result, the lath with low TF can be plastically deformed at low stress while the adjacent lath tend to resist yielding, therefore, dislocation pile-ups form against the boundaries of bainitic ferrite lath generating high localized stress values and eventually causing microcrack formation. In this respect, Fig. 6a shows a piece of evidence observed by TEM of the dislocations accumulated on the lath boundary during cycling.

Finally, with respect to the microcrack propagation, Fig. 9 shows several cracks arrested at bainite lath boundaries, block boundaries or prior austenite boundaries (which are indicated by circles). According with Rementeria et al., Kim et al. and Diaz et al. [18, 22, 23] both block boundaries and prior austenite boundaries are strong barrier to crack propagation and control the crack deflection. Moreover, it is important to note that the film-like retained austenite between laths or blocks can inhibit microcrack propagation since when the microcrack meets the phase boundary would need more energy to pass through the phase boundary. However, in this steel, it was also observed microcracks on trace slip planes that coalesced into a long crack (Fig.9a. f_1, f_2 and f_3). Zhai et al. [24] considered that grain boundaries can act as strong or weak barriers depending of twist (α) and tilt (β) angles of the crack plane deflection at a grain boundary (Fig. 11). This model suggests that if the twist angle and the tilt angle between crack plane and the slip plane of neighboring grain are small then the resistance of the grain boundary against crack propagation will be lower. Therefore, to analyze the crack propagation the angles α and β were calculated between crack planes corresponding to f_1, f_2 and f_3 microcracks represented in Fig. 9a. From these calculations we obtained that the angles between f_1

and f_2 have low values, corresponding with α= 3º and β= 6º indicating, according to Zhai's model, crystallographic propagation from f_1 to f_2. On the contrary, between f_3 and f_2 the angles are high (α= 30º and β= 20º) indicating that the block boundary acts as strong barrier to microcrack propagation. In fact, f_3 as well as f_2 were arrested in the boundary producing a high stress concentration, ending in a non-crystallographic coalescence of microcracks. Consequently, the tilt and twist angles are important factors to consider the crack propagation between adjacent bainitic ferrite laths

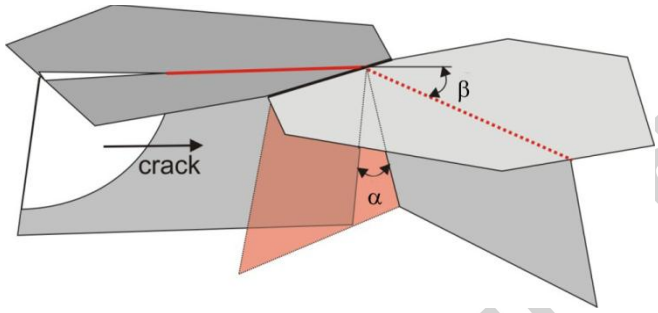

Figure 11: Zhai's model representing the twist (α) and tilt (β) angles of the crack plane deflection at a grain boundary.

5. Conclusion

In the present paper the cyclic deformation mechanisms and initiation and propagation cracks were studied during low cycle fatigue in a bainitic steel 16CrMnV7-7. The study was carried out at $\Delta\varepsilon_p$= 0.2% corresponding with the intermediate plastic strain amplitude and the results were compared with that obtained to high strain amplitude of $\Delta\varepsilon_p$ = 0.3%. The main conclusions are detailed below:

- At $\Delta\varepsilon_p$= 0.2%, the characteristic dislocation arrangement corresponds to heterogeneous distribution of loop patches of dislocations within the bainitic ferrite laths and in some laths a dislocation arrangement in form of ill-formed cells. On the other hand, at $\Delta\varepsilon_p$ = 0.3% the characteristic dislocation structure is well formed cells.

- The initial cyclic hardening is attributed to interaction of preexisting dislocations with cementite particles producing different pinning mechanism, whereas the cyclic softening is produced due to the annihilation and redistribution of the dislocations from loop patches of dislocations to cell structure.

- Microcracks nucleate in the bainitic ferrite laths on the primary slip system {110}[111] with the highest Schmid Factor and low Taylor Factor. Alternatively, the microcracks can also nucleate between bainitic ferrite laths or blocks highly misorientated

- The misorientation angles (tilt/twist) between slip planes of adjacent bainitic ferrite laths are important parameter controlling crack propagation.

Acknowledgments

This work was supported by the Bilateral Project between Argentina and Germany CONICET-DFG Res. 992/12 - Consejo Nacional de Investigaciones Científicas y Técnicas – Argentina (CONICET) and Deutsche Forschungsgemeinschaft (DFG).

References

[1] F.G. Caballero, M.J. Santofimia, C. Garcia-Mateo, J. Chao, C. Garcia de Andres, Theoretical design and advanced microstructure in super high strength steels, Mater. Des. 30 (2009) 2077–2083.

[2] H. Beladi, Y.Adachi, I. Timokhina, P.D. Hodgson, Crystallographic analysis of nanobainitic steels, Scr. Mater.60 (2009) 455-458.

[3] F.G. Caballero, H.K.D.H. Bhadeshia, Very strong bainite, Curr Opin Solid State Mater Sci. 8 (2004) 251-257.

[4] C. Garcia-Mateo, F.G. Caballero, H.K.D.H. Bhadeshia, Acceleration of low-temperature bainite, ISIJ International. 43, nº11 (2003) 1821-1825.

[5] F.C. Zhang, T.S. Wang, P. Zhang, C.L. Zheng, B. Lv, M. Zhang, Y.Z. Zheng, A novel method for the development of a low-temperature bainitic microstructure in the surface layer of low-carbon steel, Scr. Mater. 59 (2008) 294-296.

[6] T.S. Wang, X.Y. Li, F.C. Zhang, Y.Z. Zheng, Microstructures and mechanical properties of 60Si2CrVA steel by isothermal transformation at low temperature, Mater Sci Eng. A 438–440 (2006) 1124–1127.

[7] F. García Caballero, M. J. Santofimia, C. Capdevila, C. García-Mateo, C García de Andrés, Design of Advanced Bainitic Steels by Optimisation of TTTDiagrams and T_0 Curves, ISIJ Int, 46, nº 10 (2006) 1479–1488.

[8] R. Rementeria, I.García, M.M.Aranda , F.G.Caballero, Reciprocating- sliding wear behavior of nanostructured and ultra-fine high-silicon bainitic steels, Wear 338-339 (2015) 202–209

[9] F.C. Zhang, X.Y. Long, J. Kang., D. Cao, B. Lv, Cyclic deformation behavior of high strength carbide-free bainitic steel, Mater Des. 94 (2016) 1-8.

[10] J. Kang, F.C. Zhang, X.Y. Long, B. Lv, Low cycle fatigue behavior in a medium-carbon carbide-free bainitic steel, Mater.Sci.Eng. A 666 (2016) 88–93.

[11] M. Soliman, H. Mostafa, A.S. El-Sabbagh, H. Palkowskia, Low temperature bainite in steel with 0.26 wt% C, Mater.Sci. Eng. A 527 (2010) 7706-7713.

[12] X.Y. Long, F.C. Zhang, J. Kang, B. Lv, X.B. Shi, Low-temperature bainite in low-carbon steel, Mater.Sci.Eng. A 594 (2014) 344–351.

[13] S. K Bhambri, C. R Prasad., R. Vasudevan, Low cycle fatigue behaviour of a1Cr-Mo-V steel with bainite and ferrite microstructure. Int J Fatigue nº3,9 (1987) 239-46.

[14] S. Sankaran, V. Subramanya Sarma., K.A Padmanabhan. Low cycle fatigue behavior of a multiphase microalloyed medium carbon steel: comparison between ferrite/pearlite and quenched and tempered microstructures. Mater. Sci. Eng. A 345 (2003) 328-335.

[15] K. A. Padmanabhana. S. Sankaran, Fatigue behavior of a multiphase medium carbon V-bearing microalloyed steel processed through two thermomechanical routes. J. Mater Process Technol 207 (2008) 293–300.

[16] Q. Zhou, L. Qian, J. Meng, L. Zhao, F. Zhang, Low-cycle fatigue behavior and microstructural evolution in a low-carbon carbide-free bainitic steel. Mater Des. 85 (2015) 487–496.

[17] R. Branco, J.D. Costa, F.V. Antunes, Low-cycle fatigue behaviour of 34CrNiMo6 high strength steel, Theor. Appl. Fract. Mech. 58 (2012) 28–34.

[18] R. Rementeria, L. Morales-Rivas, M. Kuntz, C. Garcia-Mateo, E. Kerscher, T. Sourmail, F.G. Caballero, On the role of microstructure in governing the fatigue behaviour of nanostructured bainitic steels, Mater. Sci. Eng. A 630 (2015) 71-77.

[19] M.C. Marinelli, M.G Moscato, J.W Signorelli, A. El Bartali, I. Alvarez-Armas, K-S relationship identification technique by EBSD , Key Eng. Mater. 465 (2011) 415-418.

[20] M.C. Marinelli, I. Alvarez-Armas, U. Krupp, Short crack behavior during low-cycle fatigue in high-strength bainitic steel, Procedia Eng. 160 (2016) 183-190.

[21] M.N. Georgiyev, A.Yu Kaletin,Yu.N.Siminov,V.M.Schastlivtsev, Influence of stability of retained austenite on crack resistance of engineering steel. Phys. Met. Metall. 69 (1990) 110–118.

[22] S. Kim, S. Lee, Effect of grain size on fracture toughness in transition temperature region of Mn-Mo-Ni low-allow steel, Mater. Des. 85 (2015) 180-189.

[23] M. Diaz-Fuentes, A. Iza-Mendia, I. Gutiérrez, Analysis of different acicular ferrite microstructures in low-carbon steels by electron backscattered diffraction, Study of their toughness behavior, Metall. Mater. Trans. A 34 (2003) 2505-2516.

[24] T. Zhai, A.J. Wilkinson, J.W. Martin. A crystallographic mechanism for fatigue crack propagation through grain boundaries. Acta Mater. 48 (2000) 4917–4927.